第 34 卷第 1 期
2018 年 1 月

无 机 化 学 学 报
CHINESE JOURNAL OF INORGANIC CHEMISTRY

Vol.34 No.1
33-42

SnS_2/GCP(石墨烯复合粉末)微米复合材料作为锂离子电池负极材料的电化学性能

林 健 崔永福 崔金龙* 文钟晟 孙俊才*
(大连海事大学,大连 116026)

摘要:以石墨烯复合粉末为添加剂,采用一步水热法制备了一种 SnS_2/GCP 微米复合材料。在所得到的复合材料中,SnS_2 纳米片相互缠绕组成多孔球状 SnS_2 颗粒,石墨烯复合粉末均匀的包裹在球状 SnS_2 颗粒表面。将所制备的 SnS_2/GCP 微米复合材料用作锂离子电池负极材料测其电化学性能。结果显示,在 0.1 $A\cdot g^{-1}$ 的电流密度下可逆比容量为 795.6 $mAh\cdot g^{-1}$,循环 100 次后比容量损失不到 1%。相比于 SnS_2 其比容量和循环稳定性得到了明显改善,主要是由于石墨烯复合粉末的加入,不仅缓解了 SnS_2 颗粒在充放电过程中的团聚和体积膨胀,而且还提高了 SnS_2 颗粒的电导率。

关键词:锂离子电池;二硫化锡;负极材料;石墨烯复合粉末
中图分类号:O614.43+2 **文献标识码**:A **文章编号**:1001-4861(2018)01-0033-10
DOI:10.11862/CJIC.2018.019

Electrochemical Performance of SnS_2/GCP (Graphene Composite Powder) Microcomposite as Anode Material for Lithium-Ion Battery

LIN Jian CUI Yong-Fu CUI Jin-Long* WEN Zhong-Sheng SUN Jun-Cai*
(*Institute of Materials and Technology, Dalian Maritime University, Dalian, Liaoning* 116026, *China*)

Abstract: SnS_2/GCP (graphene composite powder) microcomposite was synthesized through a facile one-pot hydrothermal method. Graphene composite powder was used as an additive in the SnS_2 synthesis process. In the resulting SnS_2/GCP microcomposites, the sphere-like SnS_2 particles were made of several intertwining SnS_2 nanosheets accompanied by the formation of many pores on the surface of it and GCP was homogeneously anchored on SnS_2 particles. When tested as anode material for lithium-ion batteries, the SnS_2/GCP microcomposites showed a larger specific capacity (795.6 $mAh\cdot g^{-1}$ at a current density of 0.1 $A\cdot g^{-1}$) and remarkable cycling stability (less than 1% capacity loss after 100 cycles) compared with pure SnS_2. This superb energy storage performance could be mainly attributed to the existence of GCP that could not only prevent SnS_2 particles from aggregating, but also mitigate the volume changes of SnS_2 particles during charge/discharge cycle. Otherwise, the GCP could also ameliorate the electric conductivity of the SnS_2 particles.

Keywords: lithium-ion battery; SnS_2; anode material; graphene composite powder

0 Introduction

Lithium-ion batteries (LIBs) have been widely utilized in portable electronic devices, electric vehicles and plug-in hybrid electric vehicles owing to their high energy density, light weight and remarkable cycling performance[1-2]. For anode materials, current commercial graphite anodes for LIBs have a

收稿日期:2017-02-17。收修改稿日期:2017-08-28。
国家自然科学基金(No.51479019,21476035);中央高校基本科研业务费(No.3132016341)资助项目。
*通信联系人。E-mail:sunjc@dlmu.edu.cn; jinlong_cuiyuan@hotmail.com

theoretical capacity of 372 mAh·g^{-1}, which cannot meet the increasing requirement for LIBs with better electrochemical properties[3-4]. Therefore, significant efforts have been devoted to explore advanced anode materials with higher capacity, super cycle stability and better rate capability, as well as lower cost[5]. Among various anode materials, tin-based anode materials have aroused widespread concern because of their high theoretical reversible capacity (987 mAh·g^{-1})[4-6]. Among Sn-based materials, Sn metal and SnO_2 have been extensively studied[7-10]. In addition, transition metal sulfides, such as MoS_2[11], CoS_2[12], CuS[13], NiS_2[14], have been broadly investigated as promising anode materials for LIBs, owing to their high specific capacity, safety, low cost and effortless synthesis[11-14]. SnS_2 has a typical layered CdI_2-type crystalline structure in which Sn atoms are sandwiched between two layers of hexagonally compactly arranged S atoms, and the adjacent S layers are connected with weak van der Waals forces[15]. This specialized crystalline structure is conducive to intercalation of lithium-ions (Li-ions) and hence many researchers have made great efforts to synthesize SnS_2 with different structures as alternative anode materials[16-17].

Nevertheless, the practical usage of stannum sulfide for LIBs is severely hampered by remarkable volume change that occurs during Li-ions insertion and extraction reactions. It usually causes the aggregation and pulverization of active material particles with fast capacity fading[18]. Consequently, various efforts have been devoted to solving this problem by using SnS_2 nanostructured particles, such as nanoplates[19-20] and nanosheets[21], hollow spheres[22], and hierarchical structures[17], as well as 3D-hierarchical structures[15-16]. These structures could reduce absolute local volume changes and shorten charge transfer pathway, both of which can undoubtedly contribute to improving electrochemical Li-ions storage performance of SnS_2 electrodes[23]. Another specifically effective approach is to fabricate composites of metal sulfides with carbonaceous materials, such as C[24-25], graphene[26-30] or carbon nanotube[31], which not only improves the conductivity, but also buffers the mechanical stress induced by volume change[32]. Among these carbonaceous materials, graphene has become the spotlight in LIBs because it owns several desirable features, including superior electrical conductivity, excellent mechanical flexibility, large surface area, and high thermal and chemical stability[33-34]. Forming a composite with graphene has been proven to be a useful strategy to improve the cycling stability of SnS_2 electrodes[26-30]. The flexible graphene nanosheets act not only as a buffer to accommodate the volume changes during conversion reactions, but also as a separator to prevent the particles from aggregating upon long life cycling[35]. Even so, the high price of graphene increases the production cost of SnS_2/Graphene electrodes[36].

In order to reduce the production cost of SnS_2/graphene electrodes, graphene composite powder (GCP) was chosen to substitute graphene as an additive in the SnS_2 synthesis process. GCP is mainly composed of graphene (46.5%, weight percent) and conductive carbon black (46.5%) (Table 1), so it is much cheaper than graphene. In this work, SnS_2/GCP microcomposites were synthesized via a facile one-pot hydrothermal approach using stannic chloride ($SnCl_4·5H_2O$) and thiourea (CH_4N_2S) as starting materials in the presence of GCP. The resulting SnS_2/GCP microcomposites were composed of SnS_2 particles intertwined with the interconnected GCP and GCP was uniformly coated on the surfaces of SnS_2 particles. This unique morphology gave rise to the synergistic effect between SnS_2 and GCP, which was contributed to an improved specific capacity, high rate capability,

Table 1 Characteristics of graphene composite powder (GCP)

Main constituents (weight percent) / %	
Graphene	46.5±0.2
Conductive carbon black	46.5±0.2
Polymeric dispersant	7±0.2
Moisture	≤0.5
Ash	≤0.05
Physical properties	
Average thickness of grapheme / nm	2.4
Graphene sheet size / μm	5~15
Apparent density / (g·cm^{-3})	0.10
Conductivity / (S·cm^{-1})	40

as well as outstanding cycle stability up to 400 cycles.

1 Experimental

1.1 Materials

All reagents used in the synthetic process were analytical grade without further purification. Graphene composite powder (GCP) (GC1-Powder 4lib) was supplied by Ningbo Mexi Technology Co. Ltd. The characteristics of GCP are listed in Table 1. Distilled water was employed in all synthesis process.

1.2 Preparation of SnS_2/GCP

For preparation of SnS_2/GCP microcomposite, 0.3 g GCP was dispersed in 40 mL deionized water with ultrasonic to form a homogeneous GCP dispersion. 3.5 g $SnCl_4 \cdot 5H_2O$ and 2.25 g CH_4N_2S were dissolved into 20 mL deionized water with ultrasonic to obtain 0.5 mol $\cdot L^{-1}$ $SnCl_4$ and 1.5 mol $\cdot L^{-1}$ CH_4N_2S solution, respectively. Then, these two solutions were added dropwise to the above GCP dispersion with buret under continuously stirring orderly. After vigorously stirring for another 0.5 h, the mixed dispersion was transferred to a 150 mL Teflon-lined stainless steel autoclave and heated in an electric oven at 200 ℃ for 24 h. Finally, the autoclave was allowed to cool down to room temperature naturally. The resulting precipitate was collected by vacuum filtration and washed several times with deionized water and ethanol, and finally dried at 80 ℃ in vacuum overnight. As a comparative experiment, SnS_2 was prepared under the same condition without adding GCP.

1.3 Characterizations

The X-ray diffraction (XRD) (RigakuD/MAX-3A, Rigaku Corporation, Japan) patterns of pure SnS_2, GCP and SnS_2/GCP microcomposite were obtained using a Co $K\alpha$ radiation (λ=0.154 06 nm) at operating voltage of 40 kV and a filament current of 40 mA. The diffraction angle was scanned from 10° to 90° with a rate of 4° $\cdot min^{-1}$. Raman spectra of them were obtained via a T64000 triple Raman system (HORIBA Jobin Yvon, France) with a 532 nm Ar-ion laser. The morphology of pure SnS_2 and SnS_2/GCP microcomposite was observed using a field emission scanning electron microscope (FE-SEM) (SUPRA 55 SAPPHIRE, CARL ZEISS, Germany) and the elements distribution of SnS_2/GCP microcomposite was measured via an energy-dispersive X-ray analysis spectrometer (EDS) (X-Max, OXFORD, UK) adjunct to the SEM. Further morphological and structural investigations of SnS_2/GCP microcomposite were identified by high-resolution transmission electron microscopy (HRTEM) and selected area electron diffraction (SAED) on a JEOL JEM-2100 microscope system operated at 200 kV. The thermogravimetric measurement (TG) was carried out with a Mettler STARe thermal analyzer in a temperature range of 25 ~900 ℃ under an air atmosphere at a heating rate of 10 ℃ $\cdot min^{-1}$.

1.4 Electrochemical measurements

The electrochemical properties of the products were tested using CR2025-type coin cells. The working electrodes were prepared by mixing active materials, polyvinylidene fluoride (PVDF) and acetylene black at a mass ratio of 80∶10∶10 in NMP solvent to form a slurry. The obtained slurry was uniformly pasted on a thin copper foil and then dried at 80 ℃ under vacuum overnight. Mass loading of active material on the collector is 1.8 ~2.3 mg $\cdot cm^{-2}$. The electrodes were then assembled into half cells in an Ar-filled glove box using Li foil as a counter electrode, polypropylene microporous sheet (Celgard 2400) as a separator and Ni foam as a filler. 1 mol $\cdot L^{-1}$ $LiPF_6$/EC+DMC (1∶1 in volume) solution was applied as the electrolyte. Galvonostatic charge/discharge was measured on a LAND-2100 (Wuhan, China) battery tester in the voltage window of 0.01~3.0 V versus Li/Li^+. Cyclic voltammetry (CV) was performed on a CHI660D electrochemical station (CHI Instrument) at a scan rate 0.05 mV $\cdot s^{-1}$ with a voltage range of 0.01~3.0 V. Electrochemical impedance spectroscopy (EIS) measurements were carried out using the CHI660D electrochemical station in a frequency range from 100 kHz to 0.01 Hz at open circuit potential with an amplitude of 10 mV.

2 Results and discussion

2.1 Physicochemical properties

The XRD patterns of GCP, SnS_2 and SnS_2/GCP

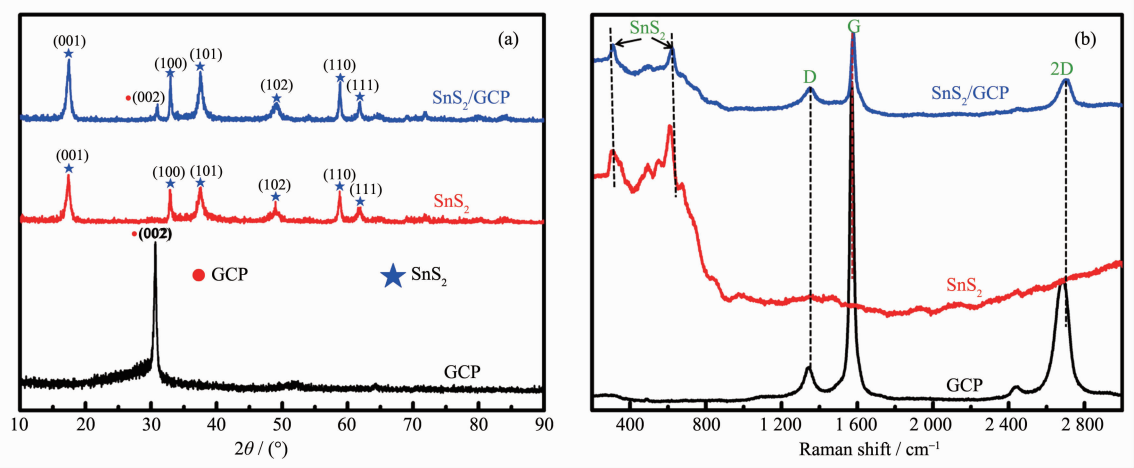

Fig.1 (a) XRD patterns and (b) Raman spectra of GCP, SnS_2 and SnS_2/GCP microcomposite

microcomposite are shown in Fig.1a. For pure SnS_2, the sharp diffraction peaks at about 17.47°, 32.865°, 37.483°, 49.048°, 58.733°, and 61.749° can be indexed to (001), (100), (101), (102), (110) and (111) planes of orthorhombic phase (PDF, No.23-0677)[28]. The obtained SnS_2/GCP microcomposite shows a similar XRD pattern to pure SnS_2, suggesting that the introduction of GCP does not influence the fabrication of SnS_2. The only peak for GCP at about 30.732° is observed, which corresponds to the (002) reflection of graphene and obvious peak related to GCP in the SnS_2/GCP microcomposite is also observed. In addition, the intensity of the diffraction peak for GCP is weaker, which confirms the higher content of SnS_2 in the hybrid structure (Fig.1a). As shown in Fig.1b, Raman spectrum of pure SnS_2 exhibits an peak at about 311 cm^{-1}, which is attributed to the A_{1g} mode according to the group theory analysis conducted by previous studies[25,37]. Moreover, a wide peak between 450 and 650 cm^{-1} could also be observed in pure SnS_2, which may be attributed to second-order effects[37-38]. In the Raman spectrum of GCP, the peak at about 1 586 cm^{-1} (G band), corresponding to an E_{2g} mode of graphitic sheets, is related to the vibration of the sp^2-bonded carbon atoms in a two dimensional hexagonal lattice[39]. While, the peak at about 1 327 cm^{-1} (D band) can be assigned to the scattering of the A_{1g} mode associated with sp^3-bonded disorder carbon, which is related to the defects or disorder in the hexagonal graphitic layers and the existence of disorder conductive carbon black[40]. Furthermore, there is another intense peak at about 2 700 cm^{-1} generally named 2D in the Raman spectrum of GCP, which is the second order of zone-boundary phonons[41]. All the peaks of both pure SnS_2 and GCP could be observed in the Raman spectrum of SnS_2/GCP microcomposite, confirming that this microcomposite is constituted of SnS_2 and GCP (Fig. 1b). Besides, the intensity ratio of the D band to the G band (I_D/I_G) for GCP is much smaller than that of SnS_2/GCP microcomposite, which can be attributed to the widely separated graphene layers promoted by the intercalation of SnS_2 nanosheets[42].

To further determine the SnS_2 content in SnS_2/GCP microcomposite, the SnS_2/GCP microcompo-site was characterized by thermogravimetric analysis (TG) as shown in Fig.2. Two stages of weight loss are seen in the TG curve of SnS_2/GCP sample. At first, an apparent weight loss of about 21.5% in the tempera-

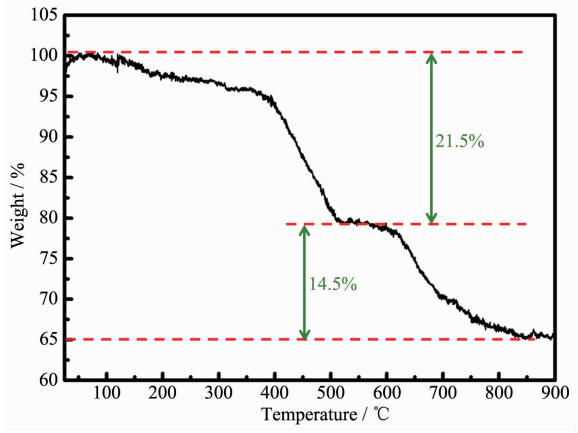

Fig.2 TG curve of SnS_2/GCP microcomposite

ture range of 40~500 ℃ is observed, which may be due to the phase conversion from SnS_2 to SnO_2[27]. The second weight loss is about 14.5% in the temperature range of 500~900 ℃, which can be attributed to the combustion of GCP. In other words, the weight fraction of GCP in SnS_2/GCP microcomposite is calculated to be 14.5%. After attaining 900 ℃, the content of remaining SnS_2 is about 64% in the mixture material.

2.2 Morphology and structure characterization

As shown in Fig.3a, the SnS_2/GCP microcomposites are constituted of SnS_2 particles with sphere-like morphology homogeneously coated by the interconnected GCP. GCP coatings act as flexible and conductive matrix to support the SnS_2 particles, forming three dimensional conductivity network for transportation of Li-ions and alleviates the volume change of SnS_2 particles[43]. Furthermore, the sphere-like SnS_2 particle is made of several intertwining SnS_2 nanosheets accompanied by the formation of many pores on the surface of it (the inset in Fig.3a). Such a porous structure could provide the efficient transport pathways to their interior voids, which could reduce Li-ions diffusion path length and lighten the volume change and mechanical strains[44]. Furthermore, this porous structure of SnS_2 particles could also increase the electrode-electrolyte interfacial area, facilitating electrochemical reactions and supplying more available Li-ions storage sites [45]. Thereupon, these structure characterizations would assure the excellent electrochemical performance of the SnS_2/GCP electrode[46-47]. EDS mapping images from SEM show that C, S and Sn elements have a relatively uniform distribution, manifesting the good contact between SnS_2 particles and GCP coatings (Fig.3b). It is contributed to not only improving electrical conductivity of the SnS_2 particles, but also effectually preventing the aggregation of them during Li-ions insertion and extraction[3,47]. The TEM image of SnS_2/GCP microcomposite demonstrates once again that the SnS_2 particles are coated by the interconnected GCP (Fig. 3c). The SAED patterns of SnS_2/GCP microcomposite

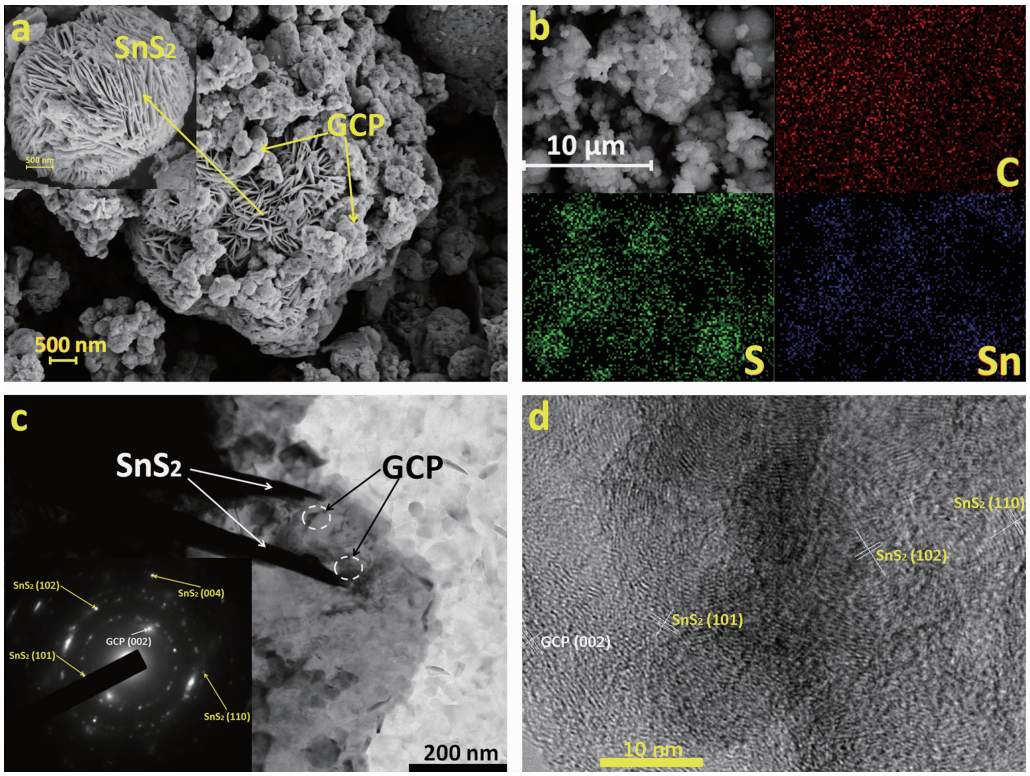

Fig.3 FE-SEM images of (a) SnS_2/GCP microcomposite and SnS_2 (inset); (b) EDS mappings of C, S and Sn elements of SnS_2/GCP microcomposite; (c) TEM image and SAED patterns (inset) and (d) HRTEM image of SnS_2/GCP microcomposite

(the inset in Fig.3c) show that the diffraction spots of it could be placed in five concentric rings. The lattice plane spaces calculated from these rings are in line with SnS_2 (101), (102), (110) and (004), as well as GCP (002)[48]. As shown in Fig.3d, the measured *d*-spacing values of this composite are approximately 0.278 nm, 0.215 nm, 0.182 nm and 0.335 nm, which could be associated with the crystalline planes of SnS_2 (101), (102), (110) and GCP (002), respectively. These results are completely in conformity with the XRD analyses.

2.3 Electrochemical performance

Cycle voltammetry curves of SnS_2 and SnS_2/GCP electrode were measured between 0.01 and 3.0 V at a scan rate 0.05 mV·s^{-1}, as shown in Fig.4a and b, respectively. For SnS_2, the broad peaks at about 1.15 and 0.8 V during the first cathodic scan could be assigned to the conversion of SnS_2 to Sn ($SnS_2+4Li^++4e^- \rightarrow Sn+2Li_2S$)[27], and the formation of solid electrolyte interface (SEI), respectively, which should be responsible for the first irreversible capacity loss (Fig.4a). Otherwise, the peak below 0.5 V can be totally due to the formation of Li_xSn alloy ($Sn+xLi^++xe^- \rightleftharpoons Li_xSn$ ($1 \leqslant x \leqslant 4.4$))[28]. The anodic peak at about 0.7 V could be attributed to the delithiation reaction of Li_xSn alloy[32]. As for the CV curves of SnS_2/GCP electrode, the cathodic peak becomes weak and shifts from 1.2 to 1.6 V during the second cycle, which can be attributed to the weak conversion reaction of SnS_2 caused by the recomination of Sn^{4+} and S^{2-} with Li during the first cycle[26]. In addition, the cathodic peak at 0.01~0.5 V could be assigned to the formation of Li_xSn alloys and the Li-ions insertion into graphene nanosheets[26]. The anodic peaks at about 1.8 and 2.15 V might be originated from the oxygenation of generated Sn at higher potential in the charged stage[28]. The additional anodic peaks at 0.01~0.25 V would be attributed to the Li-ions extraction from graphene nanosheets[30]. By contrast, the cycling stability of the SnS_2 electrode could be well improved after the addition of GCP.

As shown in Fig.5a, the first discharge and charge capacity of SnS_2/GCP microcomposite are 1 834.7 and 874.6 mAh·g^{-1}, so the calculated coulombic efficiency is about 47.6%. This high irreversible capacity could mainly originate from the incomplete conversion reaction[27] and the formation of SEI layer on the electrode surface[49]. It is clear that all the charge/discharge plateaus are consistent with the peaks in CV curves. In addition, the curves of the 10th and 50th cycles nearly overlap, confirming that this SnS_2/GCP electrode has excellent cycling stability (Fig.5a). In order to evaluate the effect of GCP on the electrochemical properties of SnS_2/GCP microcomposite, the discharge specific capacities of SnS_2/GCP, SnS_2 and GCP at a current density of 0.1 A·g^{-1} are displayed in Fig.5b. Obviously, the SnS_2/GCP electrode shows an improved cycling stability compared with SnS_2 electrode. After 5 cycles, a capacity of over 795 mAh·g^{-1} can be maintained till 100 cycles for SnS_2/GCP electrode. In contrary, the capacity of SnS_2 electrode sharply decays from an initial capacity of 1 507.3 to 232.2 mAh·g^{-1} after 70 cycles. Poor

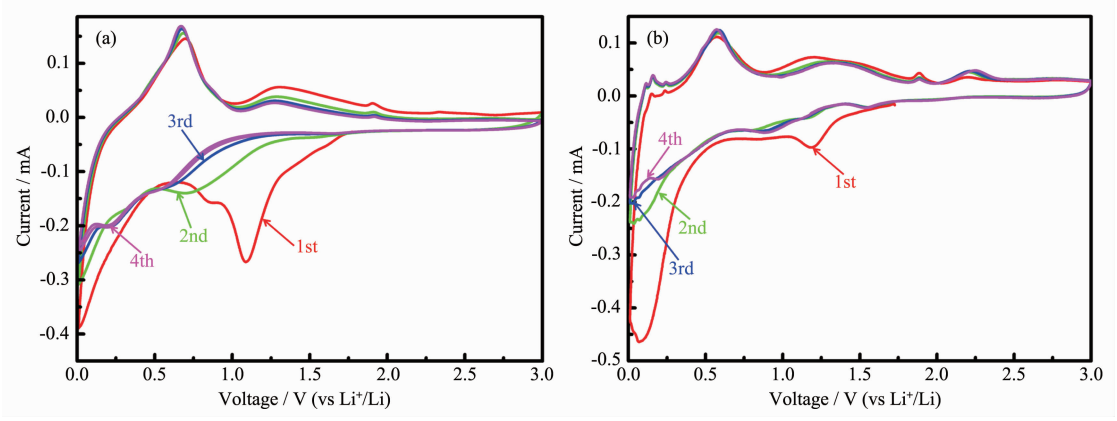

Fig.4 Cyclic voltammograms of (a) SnS_2 and (b) SnS_2/GCP electrodes at a rate of 0.05 mV·s^{-1} in a potential range of 0.01 to 3.0 V

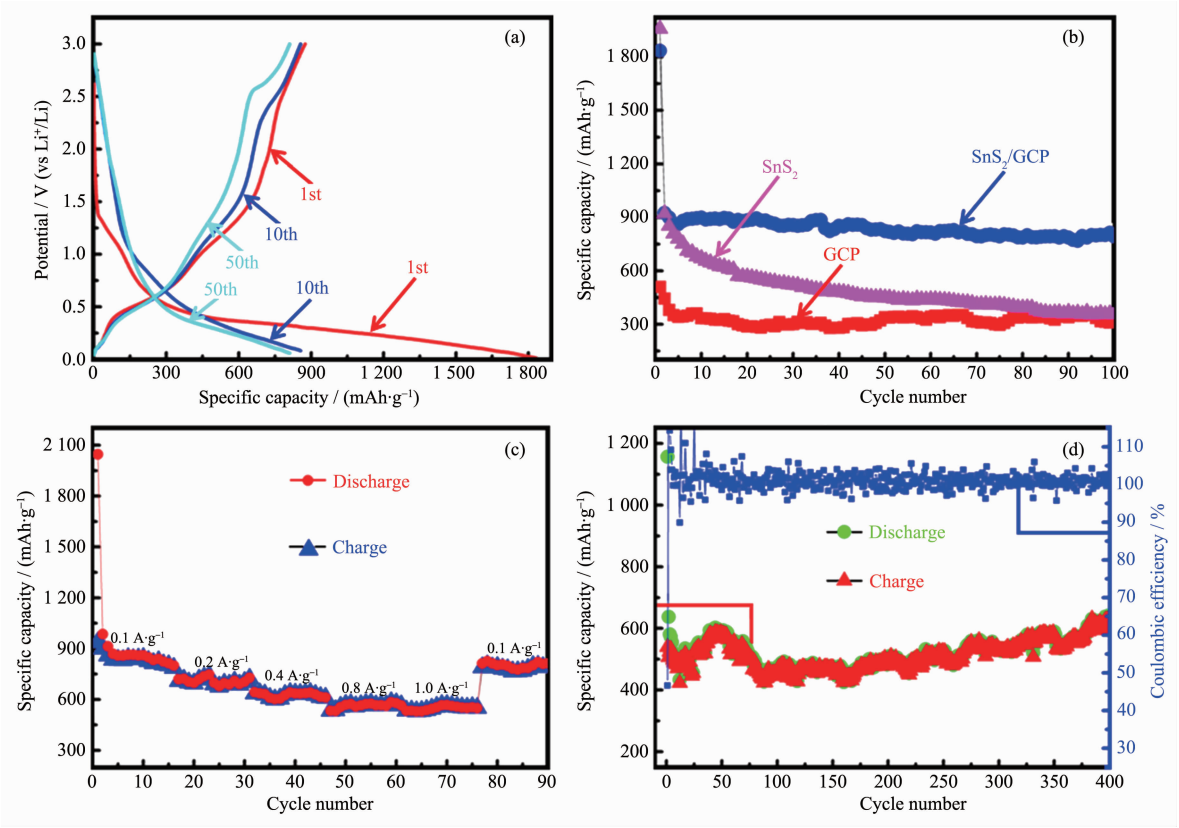

Fig.5　(a) Galvanostatic discharge/charge curves of SnS_2/GCP electrode for the 1st, 10th, and 50th cycles at 0.1 A·g^{-1}; (b) Discharge specific capacity of SnS_2/GCP, SnS_2 and GCP electrodes at 0.1 A·g^{-1}; (c) Rate capability of SnS_2/GCP electrode at 0.1, 0.2, 0.4, 0.8 and 1.0 A·g^{-1}; (d) Cycling performance of SnS_2/GCP electrode at 0.5 A·g^{-1}

cycling stability for SnS_2 electrode was also observed in the previous report[28]. In the SnS_2/GCP microcomposite, GCP coatings act as conductive and flexible matrix to support the SnS_2 particles, forming three dimensional conductivity network for transportation of Li-ions and alleviates the volume change of SnS_2 particles. Thereby, SnS_2/GCP electrode exhibits an improved capacity and superb cycling stability compared with pure SnS_2. Although GCP has an excellent cycling stability, its specific capacity is too low to be used as commercial electrode material (332.4 mAh·g^{-1}). In addition to the high reversible capacity and remarkable cycle stability, the SnS_2/GCP microcomposite also demonstrates an excellent rate capability (Fig.5c). The charge/discharge rates are programmably modified from 0.1 to 0.2, 0.4, 0.8, 1.0 A·g^{-1} and then back to 0.1 A·g^{-1} for 15 cycles. It can be observed that the discharge capacities varies from 857 to 813, 704, 615, 578, 550 mAh·g^{-1} and finally reversibly back to 825 mAh·g^{-1} at current rates of 0.1, 0.2, 0.4, 0.8, 1.0 A·g^{-1} and 0.1 A·g^{-1}, respectively. It is noted that the SnS_2/GCP electrode can still deliver a capacity of 550 mAh·g^{-1} even at the high current rate of 1.0 A·g^{-1}, which is still higher than the theoretical capacity of traditional graphite.

The cyclic performance of SnS_2/GCP electrode was tested at 0.5 A·g^{-1} with voltage range of 0.01~3.0 V, and the result is plotted in Fig.5d. Although the cyclic performance curve is slightly fluctuating, the SnS_2/GCP electrode exhibits high reversible capacity, approximately 642.8 A·g^{-1}, which is much higher than SnS_2/graphene aerogels (300 mAh·g^{-1} at 0.5 A·g^{-1})[27] and SnS_2/MWCNTs (multiwalled carbon nanotubes) hybrid (510 mAh·g^{-1} at 0.1 A·g^{-1})[31]. Table 2 lists the comparison of specific capacities of SnS_2 composite synthesized using carbonaceous materials as additive. Notwithstanding the specific capacity of SnS_2/GCP microcomposite is not the highest, the lower cost and

Table 2 Comparison of specific capacities of SnS_2 composites

Sample	Additive	Mass rate of additive / %	Current density / ($A \cdot g^{-1}$)	Capacity / ($mAh \cdot g^{-1}$)	Ref.
Carbon-coated SnS_2	Carbon	17	0.08	668	[25]
SnS_2/reduced graphene oxide	Graphene oxide	5.3	0.1	1 005	[26]
SnS_2/graphene aerogels	Graphene aerogels	14.3	0.05	656	[27]
SnS_2/graphene	Graphene	10.9	0.1	1 060	[28]
Few-layer SnS_2/graphene	Graphene	11.36	0.1	920	[29]
SnS_2@GF	Graphene foam	—	0.1	1 386.7	[30]
SnS_2/MWCNTs	Carbon nanotubes	8.9	0.1	510	[31]
SnS_2 nanoparticle/graphene	Graphene	32.1	0.1	731	[32]
SnS_2-graphene	Graphene	17.8	0.2	903	[35]
SnS_2/GCP	GCP	14.5	0.1	795.6	This work
			0.5	642.8	This work

less usage of GCP would make it widely available for commercial production. Meanwhile, the coulombic efficiency is very close to 100% all over the 400 cycles after the first cycle. The distinct behavior of SnS_2/GCP and pure SnS_2 indicates that the addition of GCP can not only prominently enhance the specific capacities of this microcomposite, but also effectively improve its cycling stabilities.

Such outstanding electrochemical properties of this resulting SnS_2/GCP microcomposite could be explained by multiple factors: (1) Although the capacity of GCP itself is not very high, the conductive GCP can provide many pathways for electrons and Li-ions and improve the whole conductivity of the composite electrode. (2) C, S and Sn elements have a relatively uniform distribution, which could effectually prevent the aggregation of SnS_2 particles during Li-ions insertion and extraction. (3) The porous structure and GCP coatings of SnS_2/GCP particles could facilitate electrochemical reactions, supply more available Li-ions storage sites and lighten the volume change and mechanical strains. These characteristics could guarantee high reversible capacity and superb cyclic stability of the resulting SnS_2/GCP microcomposite.

To explain the different electrochemical behaviors between SnS_2/GCP microcomposite and SnS_2, EIS were measured after cycling for 100 cycles as shown in Fig.6. For both electrodes, the Nyquist plots are consisted of a depressed semicircle in the high-to-middle frequency region and a slopping line in the low frequency region[50]. These plots are fitted by an equivalent circuit given in the inset of Fig.6. The semicircle in the high frequency region corresponds to the charge transfer resistance (R_{ct}) of the anode and the straight line in the low-frequency domain corresponds to the Li-diffusion process within electrodes. In addition, the intersections of the semicircle with the real axis at high frequency region (denoted as R_e) are attributed to the internal resistance, associating with electronic resistance of the anode and the ionic resistance of the liquid electrolyte[3,51]. According the fitting results, the values of R_e and R_{ct} of SnS_2/GCP electrode after 100 cycles are 35.02 and 30.85 Ω, respectively, which are lower than those of SnS_2 electrode (71.24 and 76.03 Ω). These results indicate that the addition of GCP can significantly increase the

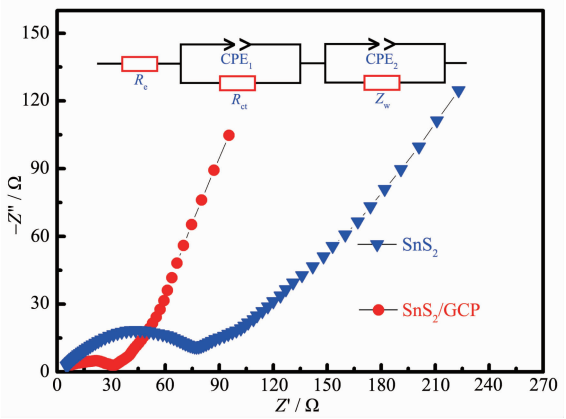

Fig.6 Nyquist plots of SnS_2 and SnS_2/GCP electrodes after 100th cycle

electronic conductivity of composite electrode and enhance rapid electron transport during the Li-ions insertion/extraction process, so the electrochemical performance of SnS_2 could be effectively improved[52].

3 Conclusions

Through the hydrothermal method, the SnS_2/GCP microcomposites which could be used as anode materials for lithium-ion batteries were effectively prepared. The resulting SnS_2/GCP microcomposites showed an impressive electrochemical performance with a specific capacity of about 642.8 $mAh \cdot g^{-1}$ and excellent cyclic stability without any degradation after 400 charge/discharge cycles at 0.5 $A \cdot g^{-1}$ in the voltage window of 0.01~3.0 V. The addition of GCP was very helpful to provide good electronic conductivity and lighten the volume change of SnS_2 particles.

References:

[1] Armand M, Tarascon J M. *Nature*, **2008**,**451**:652-657

[2] JI Wen-Xu(纪文旭), WU Di(吴迪), YANG Rong(杨蓉), et al. *Chinese J. Inorg. Chem.*(无机化学学报), **2015**,**31**(4):659-665

[3] Cui J L, Cui Y F, Li S H, et al. *ACS Appl. Mater. Interfaces*, **2016**,**8**:30239-30247

[4] PENG Peng(彭鹏), WEN Zhao-Yin(温兆银), LIU Yu(刘宇), et al. *Chinese J. Inorg. Chem.*(无机化学学报), **2014**,**30**(6):1293-1298

[5] Alias N, Mohamad A A. *J. Power Sources*, **2015**,**274**:237-251

[6] Du Z J, Zhang S C, Xing Y L, et al. *J. Power Sources*, **2011**, **196**:9780-9785

[7] Cheng Y Y, Huang J F, Li J Y, et al. *J. Power Sources*, **2016**, **324**:447-454

[8] Liu R P, Su W M, He P, et al. *J. Alloys Compd.*, **2016**,**688**:908-913

[9] Guo C, Yang Q Q, Liang J W, et al. *Mater. Lett.*, **2016**,**184**:332-335

[10]Wang F, Jiao H X, He E K, et al. *J. Power Sources*, **2016**, **326**:78-83

[11]Shu H B, Li F, Hu C L, et al. *Nanoscale*, **2016**,**8**:2918-2926

[12]Wang Q H, Jiao L F, Han Y, et al. *J. Phys. Chem. C*, **2011**, **115**:8300-8304

[13]Han Y, Wang Y P, Gao W H, et al. *Powder Technol.*, **2011**, **212**:64-68

[14]Chen Q N, Chen W X, Ye J B, et al. *J. Power Sources*, **2015**, **294**:51-58

[15]Guan D S, Li J Y, Gao X F, et al. *J. Alloys Compd.*, **2016**, **658**:190-197

[16]Zai J T, Wang K X, Su Y Z, et al. *J. Power Sources*, **2011**, **196**:3650-3654

[17]Zhu W B, Yang Y W, Ma D M, et al. *Ionics*, **2015**,*21*:19-26

[18]Duan B C, Wang W K, Zhao H L, et al. *Rare Metal Mater. Eng.*, **2012**,**41**(3):93-100

[19]Wang L Y, Zhuo L H, Yu Y C, et al. *Electrochim. Acta*, **2013**,**112**:439-447

[20]Seo J W, Jang J T, Park S W, et al. *Adv. Mater.*, **2008**,**20**:4269-4273

[21]Kim T J, Kim C, Son D, et al. *J. Power Sources*, **2007**,**167**:529-535

[22]Xia J, Li G C, Mao Y C, et al. *CrystEngComm*, **2012**,**14**:4279-4283

[23]Ara M, Wadumesthrige K, Meng T J, et al. *RSC Adv.*, **2014**, **4**:20540-20547

[24]Du Y P, Yin Z Y, Rui X H, et al. *Nanoscale*, **2012**,**5**:1456-1459

[25]Kim H S, Chung Y H, Kang S H, et al. *Electrochim. Acta*, **2009**,**54**:3606-3610

[26]Zhang Q Q, Li R, Zhang M M, et al. *Electrochim. Acta*, **2014**,**115**:425-433

[27]Jiang X, Yang X L, Zhu Y H, et al. *J. Power Sources*, **2013**, **237**:178-186

[28]Tang H L, Qi X, Han W J, et al. *Appl. Surf. Sci.*, **2015**,**355**:7-13

[29]Chang K, Wang Z, Huang G C, et al. *J. Power Sources*, **2012**,**201**:259-266

[30]Ren Y D, Lv W M, Wen F S, et al. *Mater. Lett.*, **2016**,**174**:24-27

[31]Sun H Y, Ahmad M, Luo J, et al. *Mater. Res. Bull.*, **2014**, **49**:319-324

[32]Wei W, Jia F F, Wang K F, et al. *Chin. Chem. Lett.*, **2017**,**28**:324-328

[33]Geim A K. *Science*, **2009**,**324**:1530-1534

[34]Wu Z S, Zhou G M, Yin L C, et al. *Nano Energy*, **2012**,**1**:107-131

[35]Du N, Wu X L, Zhai C X, et al. *J. Alloys Compd.*, **2013**, **580**:457-464

[36]http://www.reagent.com.cn:666/ScrcBackGroup/reagent/cpzx/cpss.jsp

[37]Wang C R, Tang K B, Yang Q, et al. *Chem. Phys. Lett.*, **2002**,**357**:371-375

[38]Julien C, Mavi H S, Jain K P, et al. *Mater. Sci. Eng. B*, **1994**,**23**(2):98-104

[39]Li N, Jin S X, Liao Q Y, et al. *Nano Energy*, **2014**,**5**:105-115

[40]Lv P P, Zhao H L, Gao C H, et al. *J. Power Sources*, **2015**, **274**:542-550

[41]Ferrari A C, Meyer J C, Scardaci V, et al. *Phys. Rev. Lett.*, **2006**,**97**:187401

[42]Luo B, Fang Y, Wang B, et al. *Energy Environ. Sci.*, **2012**, **5**:5226-5230

[43]Huang Y G, Lin X L, Pan Q C, et al. *Electrochim. Acta*, **2016**,**193**:253-260

[44]Tao H C, Huang M, Fan L Z, et al. *Solid State Ionics*, **2012**, **220**:1-6

[45]Li M Q, Zeng Y, Ren Y R, et al. *J. Power Sources*, **2015**, **288**:53-61

[46]Lin J, Cui J L, Cheng F P, et al. *J. Alloys Compd.*, **2017**, **695**:2173-2179

[47]Cui J L, Cheng F P, Lin J, et al. *Powder Technol.*, **2017**, **311**:1-8

[48]Wang Y K, Ding J, Liu Y H, et al. *Ceram. Int.*, **2015**,**41**: 15145-15152

[49]GENG Kai-Ming(耿凯明), WU Jun-Jie(吴俊杰), GENG Hong-Bo(耿洪波), et al. *Chinese J. Inorg. Chem.*(无机化学学报), **2016**,**32**(9):1495-1502

[50]Hu Y S, Demir-Cakan R, Titirici M M, et al. *Angew. Chem. Int. Ed.*, **2008**,**47**:1645-1649

[51]Tao H C, Yang X L, Zhang L L, et al. *Ionics*, **2014**,**20**:1547 -1552

[52]YANG Rong(杨蓉), LIU Xu-Wang(刘绪望), PENG Lu-Ming (彭路明). *Chinese J. Inorg. Chem.*(无机化学学报), **2017**,**33** (2):210-218